

The YAth Iranian Conference on Optics and Photonics (ICOP Y·YY), and the YEth Iranian Conference on Photonics Engineering and Technology (ICPET Y·YY).

> Shahid Chamran University of Ahvaz, Khuzestan, Iran, Feb. \-\", \'\'\\



بررسی جفتشدگی مد پلاسمونی در دو نانونوار طلا

محمدرضا حسن پور و مصطفى قربانزاده

دانشگاه حکیم سبزواری، دانشکده مهندسی برق و کامپیوتر، سبزوار

چکیده - در این مقاله، با استفاده از جفتشدگی دو نانونوار طلا، یک بستر جدیدی را برای تشخیص و تلهاندازی نانوذرات پیشنهاد می دهیم که از پلاسمونهای سطحی انتشاری تحصیر و تقویت شده با نیمرخ مد متفاوت بهره میبرد.ما با استفاده از روش تفاضل محدود مد ویژه (FDE) به بررسی مدهای پلاسمونی که مابین دو نوار طلا جفت شده تحریک می شوند، میپردازیم. ما در این بررسی نشان میدهیم که در ساختار فلز دی الکتریک فلز ارائه شده، پروفایل مدهای پلاسمونی، ضریب شکست موثر و میزان تلفات، وابستگی زیادی به ماده تشکیل دهنده عایق (محیط حسکنندگی)، ابعاد ساختار و فرکانس تابشی منبع دارد.

كليد واژه ـ پلاسمونهای سطحی، تلفات، جفتشدگی موجبر، سنسور نوری، ضريب شكست موثر.

Investigation of plasmonic mode Coupling of two Gold Nano-strips

Mohammad-reza Hasanpour and Mostafa Ghorbanzadeh

Faculty of Electrical and Computer Engineering, Hakim Sabzevari University, P.O. Box **, Sabzevar **, Y*, Iran.

m.ghorbanzadeh@hsu.ac.ir

Abstract- In this paper, by coupling two gold strips we propose a new platform for sensing and trapping nanoparticles that benefit from enhanced and confined propagating surface plasmons with different mode profiles. We study the plasmonic modes that can be excited between these two coupled gold strips by the Finite difference eigenmode (FDE) method. We show that, in this Metal-Insulator-Metal (MIM) structure, the plasmonic mode profiles, effective refractive index ($n_{\rm eff}$), and loss factor, strongly depend on insulator material (or sensing medium), the dimension of the structure, and the illuminated source frequency.

Keywords: Effective refractive index, loss, opto-sensor, surface plasmons, waveguide coupling.

1. Introduction

Plasmons are the collective motion of free electrons in metals coupled with light that makes a variety of applications at the nano-scale range [1]. Excitation of plasmons for a metal such as gold (Au) can be realized by the momentum matching technique to create a localized and enhanced field at the visible range of the light spectrum [7]. Due to subwavelength waveguiding, light concentration beyond the diffraction limit, ultrafast response, high environmental sensitivity and, flexibility in design, surface plasmons attract more attention in developing different types of sensors [7] and especially optical tweezers for example based on the propagating surface plasmons on top of a single gold strip layer [2].

In this paper, by coupling two gold strips we propose a new platform for sensing and trapping nanoparticles that benefit from enhanced and confined propagating surface plasmons with different mode profiles. We study the plasmonic modes that can be excited between two coupled gold strips by the finite difference eigenmode (FDE) method. We show that, in this Metal-Insulator-Metal (MIM) structure, the plasmonic mode profiles, effective refractive index (n_{eff}), and loss factor, strongly depend on insulator material (or sensing medium), the dimension of the structure, and the illuminated source frequency.

Y. Structure and simulation method

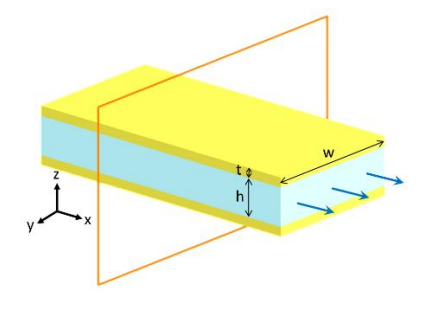


Fig. \: The structure of coupled Gold strip

The coupled gold strip waveguide is made up of three main parts including a middle dielectric layer and top and bottom gold (Au) metal layers that are shown in Fig. \. The height of the middle dielectric layer, the thickness of the metal layer, and the width of the waveguide are indicated by h and t, and w, respectively. The frequency of the source (that will be injected along the -x direction) is set to \(\forall \tau\cdot \text{THz}\) (\(\pi\lambda\gamma\gamma\gamma\gamma\gamma\gamma\gamma\gamma\gamma\gamma\gamma\gamma\gamma\gamma\gamma\gamma\gamma\gamma\gamma\gamma\gamma\gamma\gamma\gamma\gamma\gamma\gamma\gamma\gamma\gamma\gamma\gamma\gamma\gamma\gamma\gamma\gamma\gamma\gamma\gamma\gamma\gamma\gamma\gamma\gamma\gamma\gamma\gamma\gamma\gamma\gamma\gamma\gamma\gamma\gamma\gamma\gamma\gamma\gamma\gamma\gamma\gamma\gamma\gamma\gamma\gamma\gamma\gamma\gamma\gamma\gamma\gamma\gamma\gamma\gamma\gamma\gamma\gamma\gamma\gamma\gamma\gamma\gamma\gamma\gamma\gamma\gamma\gamma\gamma\gamma\gamma\gamma\gamma\gamma\gamma\gamma\gamma\gamma\gamma\gamma\gamma\gamma\gamma\gamma\gamma\gamma\gamma\gamma\gamma\gamma\gamma\gamma\gamma\gamma\gamma\gamma\gamma\gamma\gamma\gamma\gamma\gamma\gamma\gamma\gamma\gamma\gamma\gamma\gamma\gamma\gamma\gamma\gamma\gamma\gamma\gamma\gamma\gamma\gamma\gamma\gamma\gamma\gamma\gamma\gamma\gamma\gamma\gamma\gamma\gamma\gamma\gamma\gamma\gamma\gamma\gamma\gamma\gamma\gamma\gamma\gamma\gamma\gamma\gamma\gamma\gamma\gamma\gamma\gamma\gamma\gamma\gamma\gamma\gamma\gamma\gamma\gamma\gamma\gamma\gamma\gamma\gamma\gamma\gamma\gamma\gamma\gamma\gamma\gamma\gamma\gamma\gamma\gamma\gamma\gamma\gamma\gamma\gamma\gamma\gamma\gamma\gamma\gamma\gamma\gamma\gamma\gamma\gamma\gamma\gamma\gamma\gamma\gamma\gamma\gamma\gamma\gamma\gamma\gamma\gamma\gamma\gamma\gamma\gamma\gamma\gamma\gamma\gamma\gamma\gamma\gamma\gamma\gamma\gamma\gamma\gamma\gamma\gamma\gamma\gamma\gamma\gamma\gamma\gamma\gamma\gamma\gamma\gamma\gamma\gamma\gamma\gamma\gamma\gamma\gamma\gamma\gamma\gamma\gamma\gamma\gamma\gamma\gamma\gamma\gamma\gamma\gamma\gamma\gamma\gamma\gamma\gamma\gamma\gamma\gamma\gamma\gamma\gamma\gamma\gamma\gamma\gamma\gamma\gamma\gamma\gamma\gamma\gamma\gamma

In Fig. ${}^{\Upsilon}(c)$ the y-z cross-section of the waveguide is illustrated. Here, the selected values for the dimensions are ${}^{\circ} \cdot nm$, ${}^{\Upsilon} \cdot nm$ and, ${}^{\circ} \cdot nm$ for t, h, and w, respectively. In these simulations, we have only considered the first five modes which had the highest $n_{\rm eff}$. In Fig. ${}^{\Upsilon}(a)$ -(b), the vertical yellow line at the h= ${}^{\Upsilon} \cdot nm$ shows the effective index and loss factor of the waveguide by the mentioned h, w and, t values. the profile of the electric fields in both x and z directions (\mathbf{E}_x and \mathbf{E}_z), the real part, and the phase of the mentioned fields have been analyzed to distinguish and label them.

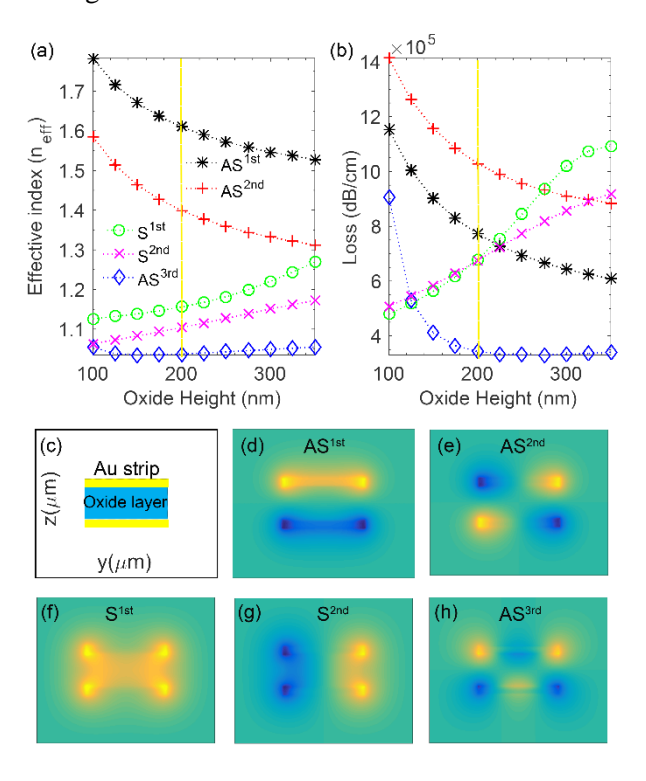


Fig. $^{\Upsilon}$: (a)-(b) Effective refractive index and loss variations with varied dielectric height h. (c) Cross-section view of MIM waveguide at the y-z plane. (d)-(h) E profiles of MIM waveguide at the y-z plane. w= $^{\circ}$ · · nm, h= $^{\Upsilon}$ · · · nm and t= $^{\circ}$ · nm

T. Simulation and Results

The observed modes have been categorized based on the symmetry of the electric field respect to the y axis at the middle of the dielectric layer, in the y-z plane. Fig. $^{\Upsilon}$ (d)-(h) respectively shows the AS $^{\prime}$ st, AS $^{\prime}$ nd, AS $^{\prime}$ nd, SS $^{\prime}$ st, and S $^{\prime}$ nd modes in which S and AS represent the Symmetric and the Anti-symmetric modes and the superscript indicates the mode number. In the following sectiones the effect of waveguide dimensions, frequency, and insulating refractive index have been investigated.

7.1 00000000 000 00000 00000 000000000

According to Fig. $^{\gamma}$ (b), it's noticeable that by increasing the oxide height h for the interval between $^{\gamma}$ and $^{\gamma}$ nm, the loss factor of the anti-symmetric modes decreases exponentially. In contrast, the loss factor of symmetric modes increase uniformly.

7,7 00000000 000 00000 00 000 000000000

of the loss of the waveguide. In this graph, the $AS^{r_{rd}}$ has the highest variation relative to all other modes.

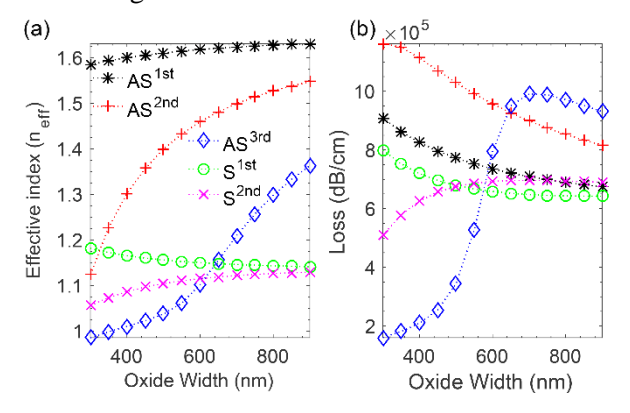
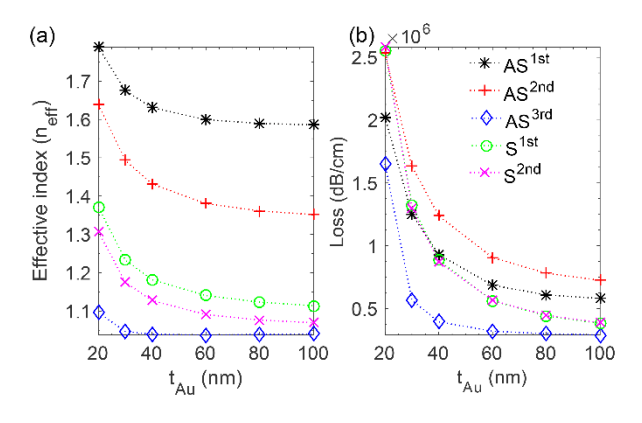


Fig. $^{\circ}$: (a)-(b) *Effective index* and *loss* variations versus w when $h=^{\circ}$ · · · nm, $t=^{\circ}$ · nm, and $w=^{\circ}$ · · · · · · · · · nm with $^{\circ}$ · · nm steps, respectively.

7,7 0000000 000 00 00000 00000000



In Fig. $\mathfrak{t}(a)$ -(b), we have demonstrated the effect of the metal layer thickness t on the n_{eff} and loss of the channel. At the frequency of \mathfrak{T} THz and constant values of h, w, and RI of the middle layer, we swept t from \mathfrak{T} to \mathfrak{T} mby \mathfrak{T} m steps. It's noticeable that the amount of the n_{eff} and loss has been decreased in all five modes over the variation interval of t. Based on the results $AS^{\mathfrak{T}}$ mode has

the highest decrease of n_{eff} by a value of \cdot , \uparrow \land \lor . In contrast, the AS $^{r_{rd}}$ mode had the lowest decay by the value of \cdot , \cdot \circ and remained approximately constant for the rest of the interval. Hence, the symmetric modes had the highest rate of decay of loss of around r , $^{r_{rd}}$ $^{r_{rd}}$ had the most rapid drop of loss for the interval of t between r $^{r_{rd}}$ and r $^{r_{rm}}$.

7,\$ 00000000 00 000 000000 0000000

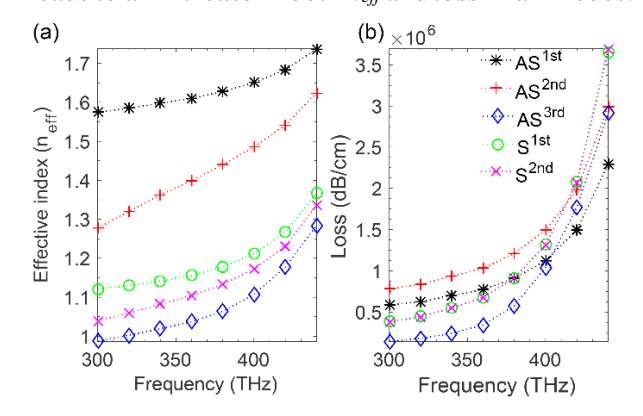


Fig. \circ : (a)-(b) Effective index and loss variations. $h=\Upsilon \cdot \cdot \cdot , t=\circ \cdot ,$ and $w=\circ \cdot \cdot \text{nm}. f=\Upsilon \cdot \cdot : \xi \cdot \text{THz}$

According to Fig. $^{\circ}$ (a), the n_{eff} of the AS^{*nd} mode has the highest rate of variation of about $^{\circ},^{\circ}$ and it has approximately a linear response in the given range of f. According to Fig. $^{\circ}$ (b), the S^{*nd} and S^{*st} modes show high sensitivity to frequency changes due to the highest variation of the *loss* parameter of about $^{\circ},^{\circ}$ (*) $^{\circ}$ (

۵۵۵۵۵ ۵۵۵۵۵ ۵۵۵ ۵۵ ۵۵ ۵۵ ۳.۵

Fig. 5 (a) illustrates the variation of n_{eff} when the refractive indices RI of sensing media changs. In this simulation, we have investigated the capability of the structure in sensing different target materials.

The *RIs* for the selected layer are 1,77, 1,50, 1,00, and 1,70 while all other parameters such as h, t, w, and f remained constant.

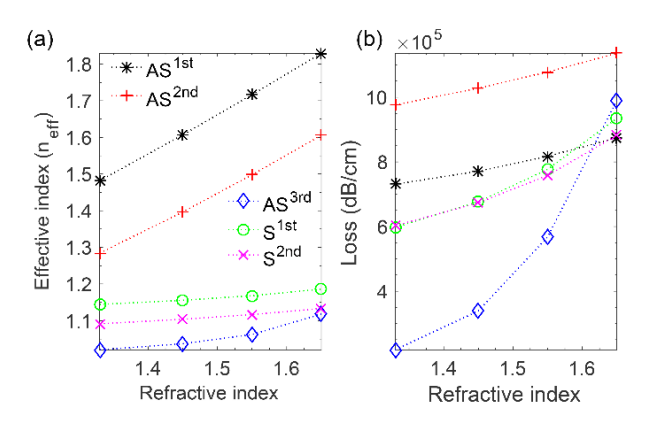


Fig. 1 : (a)-(b) *Effective index* and *loss* variations versus RI for $h=^{1}\cdots nm$, $t=^{2}\cdots nm$, $w=^{2}\cdots nm$.

F. Conclusion

According to the simulation results, for the given MIM structure, the n_{eff} and loss strongly depend on the structure geometry, dielectric material, and injection mode frequency. By utilization of the proper mode profile and geometry optimization, a high sensitive Opto-sensor can be realized.

References

- [1] V. G. Kravets, A. V. Kabashin, W. L. Barnes and A. N. Grigorenko, "Plasmonic Surface Lattice Resonances: A Review of Properties and Applications," *Chemical Reviews*, vol. 114, no. 17, pp. 0911-0901, 1014.
- [7] R. A. Alvarez-Puebla, J.-F. Li and X. Y. Ling, "Introduction to advances in plasmonics and its applications," *Nanoscale*, vol. 17, no. 17, pp. 0970-0977, 7.71.
- [*] A. I. Fernández-Domínguez, F. J. García-Vidal and L. Martín-Moreno, "Unrelenting plasmons," *Nature Photonics*, vol. 11, no. 1, pp. 1-1-1, 7-11.

The YAth Iranian Conference on Optics and Photonics (ICOP Y·YY)
The Yeth Iranian Conference on Photonics Engineering and Technology (ICPET Y·YY)
Shahid ChamranUniversity of Ahvaz, Khuzestan, Iran, Feb. Y-Y, Y·YY.

[٤] Y.-C. Lin and P.-T. Lee, "Efficient Optical Trapping of Nano-Particle via Waveguide-Coupled Hybrid

Plasmonic Nano-Taper," *IEEE Photonics Journal*, vol. ۱۱, no. ۳, pp. ۱-۱۲, ۲۰۱۹.